Sheffield Hallam University

Functionalization of metallic powder for performance enhancement

UNNIKRISHNAN, Rahul, GARDY, Jabbar, SPENCER, Ben F., KURINJIMALA, Robin, DEY, Avishek, NEKOUIE, Vahid, IRUKUVARGHULA, Sandeep, HASSANPOUR, Ali, EISENMENGER-SITTNER, Christoph, FRANCIS, John A. and PREUSS, Michael

Available from Sheffield Hallam University Research Archive (SHURA) at:

https://shura.shu.ac.uk/30430/

This document is the Published Version [VoR]

Citation:

UNNIKRISHNAN, Rahul, GARDY, Jabbar, SPENCER, Ben F., KURINJIMALA, Robin, DEY, Avishek, NEKOUIE, Vahid, IRUKUVARGHULA, Sandeep, HASSANPOUR, Ali, EISENMENGER-SITTNER, Christoph, FRANCIS, John A. and PREUSS, Michael (2022). Functionalization of metallic powder for performance enhancement. Materials & Design: 110900. [Article]

Copyright and re-use policy

See http://shura.shu.ac.uk/information.html

Sheffield Hallam University Research Archive
http://shura.shu.ac.uk

Materials & Design 221 (2022) 110900

Contents lists available at ScienceDirect

Materials & Design

journal homepage: www.elsevier.com/locate/matdes

Functionalization of metallic powder for performance enhancement

Rahul Unnikrishnan [a,*], Jabbar Gardy [b], Ben F. Spencer [a], Robin Kurinjimala [c], Avishek Dey [d], Vahid Nekouie [e,f], Sandeep Irukuvarghula [a], Ali Hassanpour [b], Christoph Eisenmenger-Sittner [c], John A. Francis [g], Michael Preuss [a]

[a] Department of Materials, University of Manchester, M13 9PL, UK
[b] School of Chemical and Process Engineering, University of Leeds, LS2 9JT, UK
[c] Institute of Solid-State Physics, Vienna University of Technology, E-138 Wiedner Hauptstrasse 8-10, 1040 Vienna, Austria
[d] Department of Chemistry, University College London, WC1H OAJ, UK
[e] Department of Materials Science & Engineering, The University of Sheffield, S9 1ZA, UK
[f] Department of Engineering & Mathematics, The Sheffield Hallam University, Sheffield S1 1WB, UK
[g] Department of Mechanical, Aerospace and Civil Engineering, University of Manchester, M13 9PL, UK

HIGHLIGHTS

- A non-stainless low alloy (SA508 Grade 3) steel powder was coated with chromium by magnetron sputtering.
- There was a significant improvement in oxidation resistance after Cr coating.
- The tribo-electric charging of powder reduced with Cr coating resulting in improved flowability.

GRAPHICAL ABSTRACT

Chromium coating on a non-stainless low alloy steel powder improved the flowability and oxidation resistance.

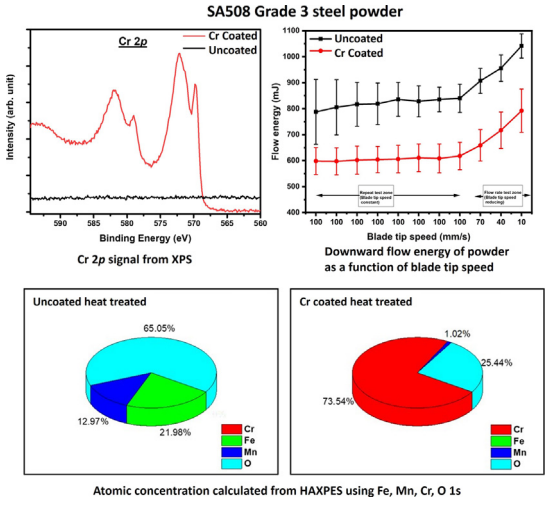

ARTICLE INFO

Article history:
Received 29 March 2022
Revised 20 June 2022
Accepted 24 June 2022
Available online 02 July 2022

Keywords:
Flowability of powder
Functionalization of powder

ABSTRACT

The oxidation state and surface properties of powder particles play a major role in the final properties of powder manufactured components. In the present study, the coating of a non-stainless low alloy (SA508 Grade 3) steel powder was explored to protect it from progressive oxidation while also studying the effects on powder flowability and electrical charging. The protective coating was applied by magnetron sputtering of chromium. The surface chemistries of both as-received and Cr coated powders were studied using X-ray photo electron spectroscopy (XPS). Accelerated oxidation tests were carried out on both uncoated and Cr coated powders to study the effects of coating on oxidation resistance. Hard X-ray photoelectron spectroscopy (HAXPES) analysis was used to measure oxygen pick up near the surface,

* Corresponding author.
E-mail address: rahul.unnikrishnan@manchester.ac.uk (R. Unnikrishnan).

https://doi.org/10.1016/j.matdes.2022.110900
0264-1275/© 2022 The Authors. Published by Elsevier Ltd.
This is an open access article under the CC BY license (http://creativecommons.org/licenses/by/4.0/).

Oxidation protection
SA508 grade 3 steel
Surface modification

showing significant reductions for the case of the Cr coated powder. The conductivity of the powder was found to increase with Cr coating. The flowability of the powder was characterised by the tapped density, the angle of repose (AOR) and a powder rheometer, and it was found to improve with a Cr coating, which can be attributed to reduced tribo-electrical charging and reduced cohesivity of the powder particles.
© 2022 The Authors. Published by Elsevier Ltd. This is an open access article under the CC BY license (http://creativecommons.org/licenses/by/4.0/).

1. Introduction

In recent years, there has been an increased interest for high performance powder based near-net-shape manufacturing techniques as they represent a cost-effective alternative to conventional manufacturing processes such as casting and forging while providing improved mechanical properties [1–4]. However, the storage and handling of powders is a major challenge in the powder metallurgy (PM) industry. Due to the large surface area of powders, one of the major challenges with metallic powder is the pick-up of oxygen, which leads to oxide inclusions when considering materials with low oxygen solubility [4–6]. Ductile fracture of metals generally occurs by nucleation, growth and coalescence of voids and hard inclusions can act as nucleation sites for such voids thereby reducing fracture toughness [7]. For the case of hot isostatically pressed (HIPed) 316L austenitic stainless steel, Adam *et al.*, [5] showed a direct correlation between the original powder oxygen content and porosities/inclusions in HIPed material. Hence oxygen pick-up needs to be kept to a minimum during powder handling and processing, especially for applications where the fracture toughness is crucial. Generally, a powder is kept in an inert atmosphere or vacuum to minimize oxygen pick-up, which makes powder storage very expensive. Irrespective of how effectively the powder is stored, there will be still some oxygen pick-up during high temperature processing as a 100% inert atmosphere is not practically achievable. For example, the oxygen concentration in 316L and SA508 steel powders are found to increase after HIPing at 1160 °C for 4 h [8]. An alternative strategy for controlling oxygen pick-up is to develop protective coatings on the powder as a part of the powder manufacturing process. It is well known that the addition of chromium to steels in sufficient quantities enables the formation of a protective Cr_2O_3 film creating a so-called stainless steel [9]. Hence, a thin chromium coating on a powder is expected to prevent its sustained oxidation during handling and storage while during solid-state processing (e.g. HIPing) or additive manufacturing processes, the thin chromium film is expected to redistribute during the high temperature procedure. Also, further oxygen content in powder can be lowered by reduction of chromium oxide during solid state processing [10].

Magnetron sputtering has been recently used to develop coatings approximately 30 nm in thickness on granular particles [11]. Even though there are many alternatives to magnetron sputtering, such as mechanical alloying [12] and electroless coating [13], these alternatives either change the spherical morphology of the powder or are less efficient on spherical powder. Also, these alternatives are less efficient when depositing a very fine coating that won't significantly change the chemical composition of the powder.

The flowability of a powder is another factor that particularly determines the reliability and quality of an additively manufactured (AM) product [14,15]. The powder flow behaviour is generally influenced by the particle size and shape, surface roughness and interactions. In particular, surface cohesion due to Van der Waals interaction can hinder powder flowability. The frictional behaviour of particles influenced by surface roughness also plays a role in powder flowability. Contact charging that results from friction leads to the transfer of electric charge between powder particles [15], which in extreme cases and for some powders can result in fire and explosion hazards during storage and transport [15,16]. Even though the electrostatic force induced by contact electrification is very small, it becomes larger than the gravitational force for very small particles [17]. This is particularly relevant for powder fusion processes where fine powder size is desired as it gives a better dimensional accuracy [14]. He *et al.*, [14] found that surface cohesion between the particles can result in the non-uniform spreading of powders and a better layering can be obtained by fine powder. The electrostatic charging properties of titania pigment particles were found to shift towards positive direction with more alumina content on the surface and towards the negative side with more silica content on the surface [17]. The magnetic properties of powder particles could also affect its flowability. However, it has been demonstrated in [18] that the magnetic effects could be reduced by degaussing the powder.

Powder surfaces can be characterised using a wide range of techniques like scanning electron microscopy (SEM), transmission electron microscopy (TEM) and X-ray photo electron spectroscopy (XPS). Even though XPS gives poor lateral spatial resolution in comparison to SEM and TEM, it is a surface sensitive technique that provides a quantitative analysis of the surface composition to depths of between 2 and 20 atomic layers [19]. An increase in X-ray photon energy increases the photoelectron kinetic energies which in turn increase the electron sampling depth (as defined by three times the inelastic mean free path of electrons). Typically Hard X-ray photoelectron spectroscopy (HAXPES) at 9 keV results in sampling depths of up to $\sim$ 50 nm, compared to 3–10 nm when using surface sensitive XPS with standard lab sources such as Al Kα [20], and therefore it enables the analysis of near surface chemistries.

To date, powder property studies have primarily focussed on improving the shape, size and particle size distribution of powders, while little attention has been paid to developing coatings that improve resistance to oxidation or the physical surface properties of powder manufactured products. The purpose of the present study is to develop Cr coatings for an SA508 Grade 3 steel powder, a metal powder that is highly sensitive to the environment as it has a low Cr content. The coating strategy pursued here was magnetron sputtering and the effects of the Cr coating were evaluated by characterising the flowability and level of oxidation of the powder with and without a coating, after different environmental exposure times, using a range of advanced characterisation tools.

2. Material and experimental work

The powder used in this study was gas atomised SA508 Grade 3 low-alloy steel powder. The bulk chemical composition of the powder was measured by inductively coupled plasma optical emission spectroscopy (for Cr, Mn, Mo, Ni, Si), combustion analysis (for C, S) and fusion analysis (for N, O) at an UKAS accredited testing facility in the UK. The chemical composition of the powder and the measurement uncertainties are given in Table 1. Fig. 1 shows as SEM image revealing the morphology of as-received powder. The particle size distribution for the as-received uncoated powder was measured by taking a series of optical microscope images at 400x magnification and using image processing software ImageJ [21] to estimate the mean diameter of individual particles. An

Table 1
Chemical composition of uncoated and Cr coated SA508 steel powder and measurement uncertainties.. P and V were below the detection limit.

Wt. %	C	Cr	Mn	Mo	N	Ni	O	P	S	Si	V	Fe
SA508 As-received	0.007	0.12	1.23	0.55	0.009	0.79	0.054	<0.005	0.006	0.25	<0.01	Bal
SA508 Cr coated	0.007	0.32	1.22	0.54	0.009	0.78	0.046	<0.005	0.006	0.25	<0.01	Bal
Uncertainty (%)	± 0.0024	± 0.014	± 0.078	± 0.018	± 0.00052	± 0.051	± 0.0052	–	± 0.0009	± 0.022	–	–

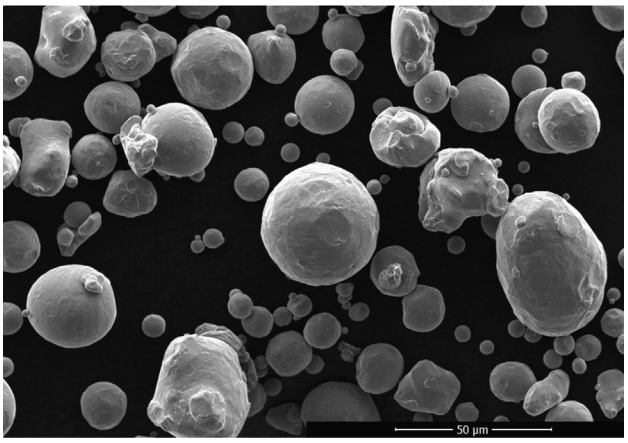

Fig. 1. SEM SE image of gas atomized as-received SA508 low alloy steel powder.

optical image of the un-coated powder is given in Supplementary result Fig. 11. The particle size distribution based on about 1000 particles is shown in Fig. 2. The mean particle diameter from the measured distribution was 9.83 ± 5 µm.

The as-received powder was coated using a custom-built magnetron sputterer at the Technical University of Vienna. Further details of the equipment can be found in [11]. Magnetron sputtering is generally done on bulk samples and for power coating a tilted rotating container was utilised [11]. Two Cr targets with 10 cm diameter were used as sources and were operated at 700 W power. Using argon as a working gas, a film growth rate of 0.6718 ± 0.0213 nm/s was achieved with a bowl tilt angle of 45° and a rotating speed of 25 rpm. Approximately 2200 g (443 ml) of SA508 steel powder was sputtered with chromium

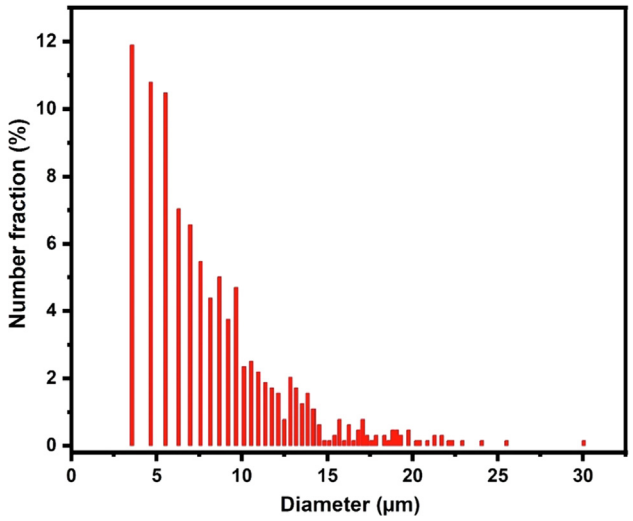

Fig. 2. Particle size distribution of gas atomized as received SA508 low alloy steel powder. This was determined by taking a series of optical microscope images and using image processing software ImageJ [21] to estimate the mean diameter of individual particles. The distribution is reported without binning.

for 8 h. Even though ferromagnetic materials are difficult to magnetron sputter [22,23], no adverse effects were detected during the coating process.

In order to accelerate the oxidation of the powder, both uncoated (AR SA508) and coated (Cr Coated SA508) steel powders were heat treated (HT) in a muffle furnace at 50 °C for 120 h. It should be noted that the primary aim of the Cr coating is to prevent/minimize oxidation of the powder during storage and handling at ambient temperature. However, in order to get significant oxidation in a shorter time period, a slightly higher temperature (50 °C) was used. The as-received uncoated powder was imaged using a field emission gun scanning electron microscope (FEG-SEM). The microstructural examination of the Cr-coated powder was carried out using a FEG-SEM equipped with an Oxford Instruments energy-dispersive X-ray spectroscopy (EDS) detector for elemental analysis. The Cr coated powder for EDS analysis was mounted in a conductive bakelite resin and ground with 4000 grit emery paper. The final polishing was done using oxide polishing suspension (OPS) for 15 min. Both SEM imaging and SEM-EDS line scans on individual particles were carried out at 10 keV.

X-ray photo electron spectroscopy (XPS) with an Al Kα monochromated X-ray source (300 W, 1486.6 eV) was used to study the surface chemistries of uncoated and Cr coated powders before and after the accelerated oxidation experiments. Hard X-ray Photoelectron Spectroscopy (HAXPES) was performed on a HAXPES-Lab, Scienta Omicron GmbH based at the Henry Royce Institute at The University of Manchester, using a Ga Kα X-ray source (250 W, 9.25 keV photon energy), which was monochromated and micro-focused to 50 µm [24,25]. The spectrometer is equipped with an EW-4000 electron energy analyser. Atomic concentrations were obtained using calculated relative sensitivity factors (RSF) for each core level [26]. Bulk oxygen measurements on the powders were carried out at an analytical testing facility using a LECO elemental gas analyser. HAXPES scans were also carried out on heat treated powders to study the effect of Cr coating on oxidation. Both XPS and HAXPES spectra were analysed using Casa XPS software [27].

The tap density of the uncoated and Cr coated SA508 grade 3 powders were measured according to the ASTM B527-20 guidelines [28]. Powder was poured into a volumetric cylinder. The cylinder was then tapped so that the powder was settled, until virtually no volume change was observed. The Hausner ratio (HR) and Carr's index (CI) were calculated from the tapped density [29,30]. The HR is calculated as

$$HR = \frac{\rho_t}{\rho_a} \tag{1}$$

where ρ_t is the tapped bulk density and ρ_a is the aerated bulk density of the powder. The Carr's Index is the ratio of the difference between the tapped bulk density and the aerated bulk density to the tapped bulk density of the powder. The CI is calculated as

$$CI = \frac{\rho_t - \rho_a}{\rho_t} \tag{2}$$

The Angle of Repose (AOR) was measured using a custom built instrument based at The University of Leeds [30]. A schematic representation of the apparatus can be found elsewhere [30]. In this

test the powder was dispensed through a funnel at a fixed height to form a conical heap on a horizontal surface. The AOR was then measured as the angle between the surface of the powder heap and the horizontal surface. The procedure was repeated 3 times and average values were taken.

A powder FT4 rheometer (Freeman Technology, Tewkesbury, Gloucestershire, UK) was used to study the flow energy of the powder. In the standard test procedure, the powder bed is initially conditioned by rotating the impeller clockwise to gently slice the bed surface and produce a reproducible, low stress packing state. The cell is then split to remove any material above a bed height. A downward test was performed, where the blade rotates anti-clockwise and penetrates the powder bed. In this way, the blade action was more compacting than slicing, resulting in shearing the bed under a normal load provided by the blade twisting angle. During the downward test, the torque (T) and axial force (F) were recorded. They were used to calculate the total combined rotational and translational work done by the blade to overcome the flow resistance of powder bed, which is termed as the 'Flow Energy', E [31]:

$$E = \int_0^H \left(\frac{T}{R\tan\alpha} + F\right) dH \tag{3}$$

where R is the radius of the blade; α is the helix angle of blade; $H = H_0\text{-}H_1$ is the penetration depth, where H_1 is the instantaneous vertical position of the blade and H_0 is the initial bed height. A glass vessel and blade with 25 mm diameter and 23.5 mm diameters, respectively, are used. In the standard downward test, the blade moves with a constant downward speed of 0.1 m/s giving a dynamic helix angle of $-5°$.

The electrical conductivity of as-received and Cr-coated powder was measured using an in-house setup based in Technical University Vienna as shown in Fig. 3 [32]. Even though the ASTM standard for measuring electrical conductivity uses International Annealed Copper Standard [33], the purpose of the electrical measurements in this work is solely to compare the trends in electrical conductivity for uncoated and Cr coated powder. The set-up in Fig. 3 consists of a moveable electrode (top) and a static counterpart (bottom), which are connected to a resistance meter. The powder sample was stored inside an acrylic glass cylinder, which is affixed at the bottom electrode. The top piston was slowly moved to compress the sample up to 1000 N while simultaneously measuring the electrical resistance. Sample sizes of 5 ml were used for each measurement, which were measured with a 5 ml measuring cylinder. A vibrating machine was used to compact the powder for measurement. Tribo-electric charging of powder was measured using a custom-built instrument which consist of a dispersion system, a Faraday cage and an electrometer based at The University of Leeds. Further details of the experimental set-up can be found in [34]. About few mm^3 of powder was fed into the dispersion unit, made of 316 stainless steel contacting surfaces. Powder was then dispersed and emptied into a Faraday cage for the charge measurement. All the measurements were performed at dispersion pressure of 4 bar against stainless steel contacting surface and the average measurement of at least 10 times repeats carried out for each sample.

3. Results and discussion

3.1. Effects of coating on the oxidation of the powder

A SEM secondary electron (SE) image of chromium coated powder along with EDS line scans for Fe and Cr spectrum are presented in Fig. 4. The EDS line scan shows higher Cr at the surface of powder after coating. However, the spatial resolution of SEM EDS line scan was not enough to measure the actual thickness of Cr coating.

The film thickness (x) from magnetron sputtering on a powder sample can be estimated as [11]

$$x = \frac{r_s R t A_{expo}}{3 V_{substrate} f f_s} \tag{4}$$

where r_s is the mean radius of the particle, R is the film deposition rate, t is the time of deposition, A_{expo} is the area exposed to the vapour beam, which is a semi empirical value that depends on the substrate volume, $V_{substrate}$ is the total volume of Cr that is deposited, f is the packing factor and f_s is the form factor. The particles were considered perfectly spherical for the calculation of film thickness. The estimated thickness of Cr coating based on the above estimate ($2r_s$ = 9.83 μm, R = 0.6718 nm/s, t = 8 h, A_{expo} = 592.69 cm^2 for 443 ml powder, $V_{substrate}$ = 443 ml, f = 0.6, f_s = 1) is approximately 7 nm. Please note that film thickness calculation is based on mean particle size of powder and hence only is a rough estimate. The chemical composition of the powder after Cr coating is given in Table 1.

High resolution XPS spectrum for (a) Fe 2*p*, (b) Mn 2*p*, (c) Cr 2*p* peaks for un-coated and Cr-coated powder is presented in Fig. 5. Fe

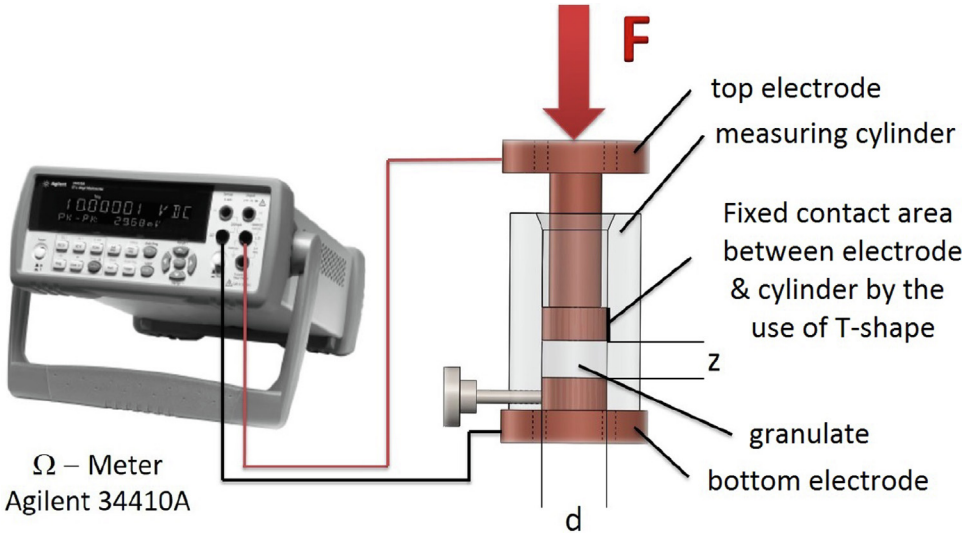

Fig. 3. Schematic of equipment used to measure the electrical resistance of granular materials as a function of applied force [32].

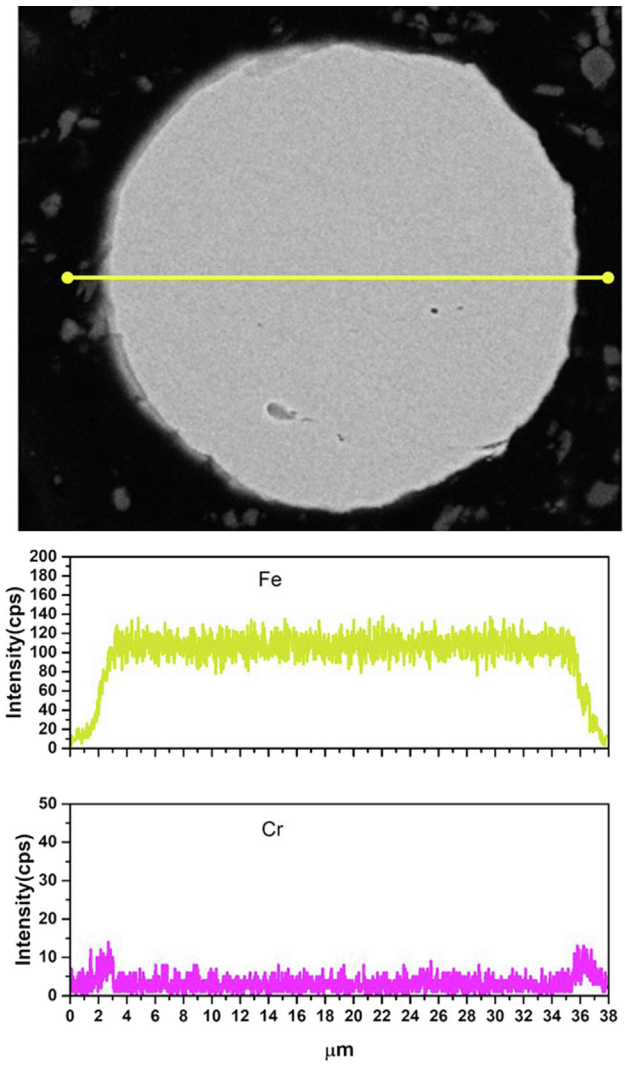

Fig. 4. SEM SE Image of Cr coated powder particle and EDS line scans of Fe and Cr across a single powder.

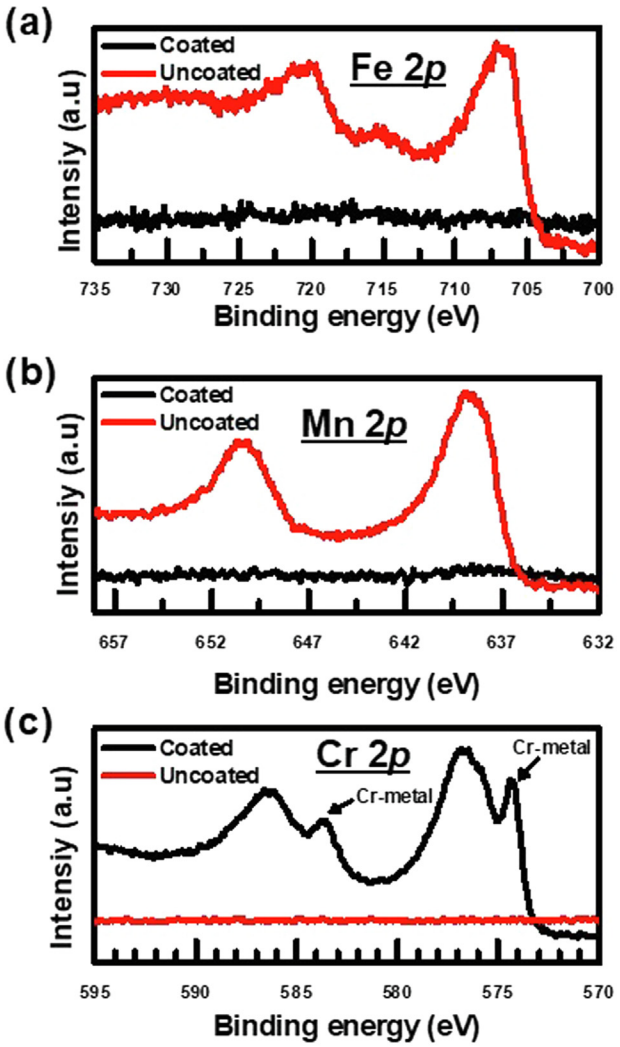

Fig. 5. Core level XP spectra of (a) Fe 2p, (b) Mn 2p, and (c) Cr 2p, for an uncoated (red lines) and coated (black lines) samples.

and Mn peaks were strong in uncoated powder whereas Cr-coated powder only showed Cr signals. The high Mn signals on uncoated powder could be due to the formation of oxides of Mn on surface due to high affinity of Mn for oxygen [35]. Since no signal from Fe or Mn on the Cr-coated powder using XPS, it could be inferred that the Cr coating completely encapsulates the steel particles; given the X-ray spot size was approximately 1 mm diameter, a large number of particles are sampled, and any gaps in the coating would have led to some Fe being detected. The sampling depth of XPS here was approximately 5 nm calculated using the well-established TPP-2 M formula [36]; given the coating was estimated to be approximately 7 nm thick, this lack of Fe signal from XPS verified the thickness is greater than 5 nm. Metallic Cr peaks were also observed in Cr 2*p* spectrum (see Fig. 5(c)) of the Cr-coated powder. Even though the repeatability of this process has not been.

In contrast, HAXPES increases the sampling depth substantially to greater than 30 nm when measuring the Fe 2*p* core level at ~ 700 eV binding energy (BE). HAXPES also enables measurement of deeper core levels, however, at much higher BE, such as Fe 1*s* (7112 eV), Cr 1*s* (5989 eV), and Mn 1*s* (6539 eV). Given these core levels are at much higher BE, the photoelectrons have lower kinetic energy (KE) and thus are associated with a reduced sampling depth, here approximately 9 nm calculated using TPP-2 M formula [36], i.e. still from a greater sampling depth than XPS but less than the maximum possible HAXPES sampling depth. Fig. 6 shows the HAXPES wide spectrum of uncoated and Cr coated powder. No Fe 1*s* or Mn 1*s* peaks were detected on Cr coated powder, but Fe 2*p* and Mn 2*p* were, indicating that the coating thickness is similar to the photoelectron sampling depth between Fe 1*s* and Fe 2*p*, thus ranging 10–20 nm. Fig. 7 shows the relative concentrations of Fe, Mn, Cr, and O, using the 1*s* orbitals for uncoated and Cr coated powder before and after heat treatment. Note that these calculations assume a thick, homogeneous material, which is not the case here, however, the relative changes between samples and treatments are still very useful. There was a reduction in oxygen on the surface of the powder after chromium coating compared to the uncoated powder (Fig. 7(a), (b)), however, the majority of the metal signal is from the Cr coating, so this amount of oxygen is now mainly associated with the coating. The oxygen levels in the uncoated powder almost doubled after accelerated oxidation heat treatment (Fig. 7(a) and (c)), whereas the oxygen levels in Cr-coated powder remained the same after the accelerated oxidation heat treatment (Fig. 7(b) and (d)).

To examine the amount of oxidized iron below the coating, the Fe 1*s* and 2*p* HAXPES spectra (Figure (8(b)) may be used. Spectra may be delineated into metallic and oxide peaks (note that the peak fitting of Fe 2*p* is perturbed by complex multiplet splitting

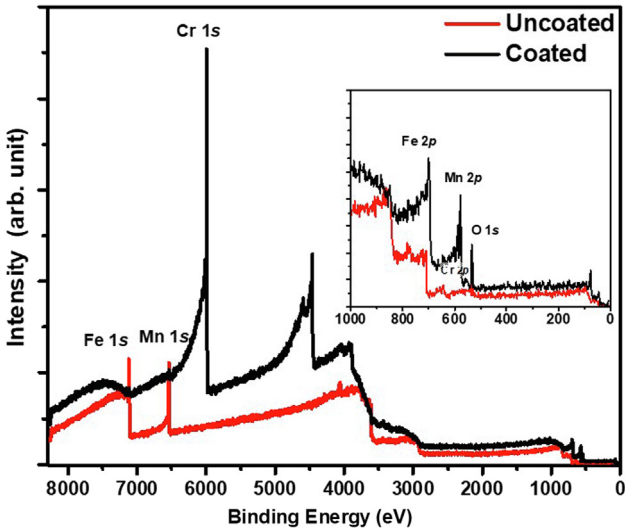

Fig. 6. HAXPES survey spectra from uncoated (black lines) and Cr-coated (red lines) SA508 powder with a zoomed in spectra for 1000-0ev.

effects, however here we simply peak fit the spectra to obtain the ratio of metallic to oxide species of the metals) [37]. Once coated, the Cr 2*s* peak is measured to lower binding energy, however the iron and manganese peaks are still measured and again the relative concentration of metallic vs. oxide may be extracted using peak fitting.

Comparing the 1*s* and 2*p* core levels, it is evident that less metallic iron and chromium are detected with the higher binding energy 1*s* core levels (Fig. 8(a) and (b)), which is again because the sampling depth is reduced, and the measurements are more surface sensitive. Note that the oxide-related core level peaks do not follow any well-established peak fitting procedure, as we are not concerned with ascertaining the particular type of oxide present, here we simply want to extract the amount of metal atoms which are oxidised in some way.

The O 1*s* spectrum in XPS is often influenced by surface contamination of carbon and carbon oxides. With HAXPES this surface contamination influences the spectra far less, and little to no carbon was detected (the carbon content in the particles is expected to be below the detection limit), and the O 1*s* spectrum showed only one symmetric peak, i.e., one chemical species associated with metal oxide at ~ 530 eV binding energy (data not shown). Using XPS would normally require deconvolution of the O 1*s* spectrum to remove the influence of surface adventitious contamination.

The Cr 2*s* was also peak fitted similarly. The Mn 1*s* peak of MnO_2 is approximately at 6541 eV [38]. The binding energy of Mn 1*s* in this study was around ~ 6540.5 eV, so, all Mn is likely present as oxide (See supplementary Fig. 12). The percentage of metallic and oxide states of Fe, Cr and Mn, at lower (1*s*) and higher (2*s*, 2*p*) sampling depth is presented in Table 2. The percentage of oxides of iron and manganese were lower in Cr coated powder compared to uncoated powder. The 2*p* and 2*s* peaks also showed lower iron oxide in the coated powder compared to uncoated powder. Further simplifying Table 2, the percent of oxide state with respect to metallic state of Cr and Fe is presented in Table 3. It is evident that more than 80% of Fe 1*s* signal is from oxide on uncoated powder whereas only 50% of Fe 1*s* signal is from oxide on Cr coated powder; 90% of the Cr 1*s* signal is from oxides on Cr coated powder and no Cr signal was detected on uncoated powder. Similar tends were observed for higher sampling depth (Fe 2*p* Cr 2*s*).

Bulk oxygen content of uncoated and Cr coated powder measured using LECO elemental gas analyser is summarised in Table 4. It can be noticed that oxygen content in Cr coated powder was

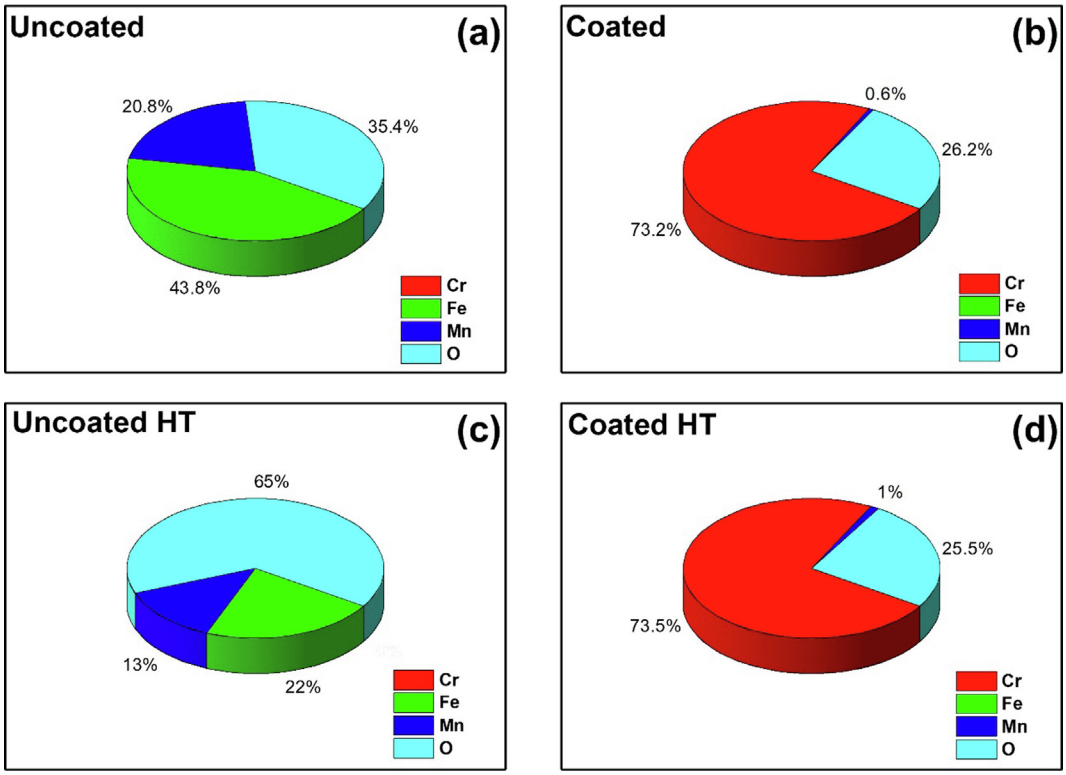

Fig. 7. Atomic concentration of (a) uncoated, (b) Cr coated, (c) uncoated heat treated and (d) Cr coated heat treated SA508 powder calculated from HAXPES using Fe, Mn, Cr, O 1s.

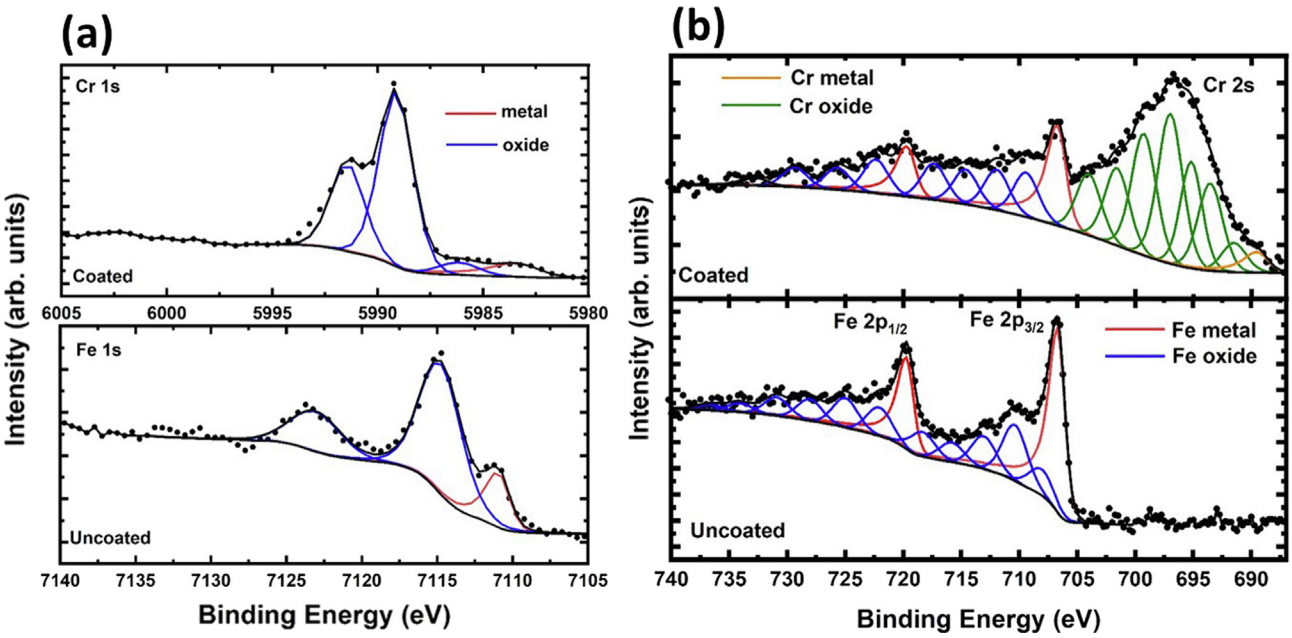

Fig. 8. (a) Cr 1s and Fe 1s HAXPES spectra, and (b) Fe 2p / Cr 2s HAXPES spectra for Cr coated (top) and uncoated (bottom) SA508 powder. Metallic and oxide species have been peak fitted. Shirley backgrounds were used throughout.

around 123 ppm lower than the uncoated powder. The powder used in the study had already have undergone some oxidation over a prolonged period. This could be the reason for a relatively high oxygen content in the Cr coated powder (447 ppm). Even though the oxygen measured from HAXPES showed a significant increase after accelerated oxidation heat treatment on the uncoated powder, the bulk oxygen measurements only increased by 24 ppm after HT. The surface of the uncoated powder comprises of iron and manganese oxides as shown by XPS data (see Fig. 5). Mn has higher diffusivity than Cr in iron based alloys thereby forming oxides of Fe and Mn which were reported to generate a less protective passivation layer in steels [39,40]. It is possible that the Fe and Mn oxides were stable in some of the powder particles as the temperature used for heat treatment in this study was only 50 °C. Also, the oxygen may have remained mostly in the near surface region (within 30 nm) for the studied temperature which was picked-up by HAXPES whereas the bulk measurements were far less sensitive. However, the bulk oxygen concentration in SA508 powder is reported to increase by 300 ppm after a full HIP cycle at 1160 °C [8]. Cr_2O_3 films are reported to form protective layer in 310 stainless steel even at temperature as high as 1000 °C [41]. Therefore, in this study, the chromium oxide film is expected to give an improved oxidation protection on SA508 powder at higher temperature compared to Mn and Fe oxide films.

3.2. Effects of Cr-coating on flowability

The tapped density, Hausner ratio (HR) and Carr's index (CI) for uncoated and Cr-coated powders are summarised in Table 5. The CI and HR was lower in coated powder compared to uncoated powder indicating a better flowability for the Cr coated powder. Angle of Repose (AOR) describes both the static and dynamic behaviour of powder [42]. AOR represents equilibrium between the kinetic energy of falling powder from the funnel and static inter-particle forces between particles that forms and maintains the heap. In this study, AOR of the powder remained unchanged after coating. The value for both coated and uncoated powder was 29 ± 0.5°. Generally, HR is found to increase with AOR [29,30]. However, in this study no relation was found between AOR and HR.

Fig. 9 shows the effect of blade tip speed on flow energy of uncoated and Cr coated powder using FT4 powder rheometer. The flow energy increased with decreasing blade tip speed for both coated and un-coated powder. It is evident that the flow energy of Cr coated powder was about 17% lower than that for the uncoated powder. As the flow energy measures the dynamic flowability of powders during the downward motion of the blade [43], we can say that the flowability of powder had significantly improved with Cr coating. Since the powder is confined in a vessel, the compressibility of the powder plays a key role in the FT4 analysis.

3.3. Electrical charging analysis

Fig. 10 shows the mean electrical resistance of uncoated and Cr coated powder as a function of applied load. The conductivity of Cr coated powder significantly increased after coating which shows change in conductivity of the particle surface. The increase in conductivity could be associated with the thickness of coating which will be lower in Cr-coated coated powder compared to that of uncoated powder. Table 6 shows electrostatic charge density of uncoated and Cr-coated SA508 powder measured using the dispersion system and Faraday cage. The charge density reduced by almost half after Cr coating. The improvement in the flowability of the coated powder could be associated with the reduced electrostatic charging of particles after coating [15,17] which in turn reduces the cohesion between powder particles. From XPS spectrum presented in Fig. 5(c), the surface of Cr coated powder comprises of chromium oxides and metallic chromium and the uncoated powder has mostly iron and manganese oxides (Fig. 5 (a), (b)) on the surface. Even though chromium oxides are generally bad conductors of electricity, sputter deposited chromium oxide films which are generally amorphous or nano crystalline in nature are reported to have conductivity up to six orders higher than bulk crystalline Cr_2O_3 films [44]. Hence, apart due to the thinner oxide layer, the presence of amorphous chromium oxide layer and metallic chromium on the surface of Cr coated powder could also have improved the conductivity and hence reduced electrostatic charging in Cr coated powder.

Table 2
Percentage of metallic and oxide peaks of Fe, Cr and Mn measured from HAXPES at lower and higher sampling depths for uncoated, Cr coated SA508 before and after heat treatment. The uncertainty represents the error's associated with peak fitting calculated from CASA XPS software.

	Cr Metal	Cr Oxide	Fe Metal	Fe Oxide	Mn Oxide	Cr Metal	Cr Oxide	Fe Metal	Fe Oxide
	Lower sampling depth (9 nm)					Higher sampling depth (30 nm)			
	Cr 1*s*		Fe 1*s*		Mn 1*s*	Fe2*p* Cr2*s*			
AR SA508	0	0	11.8 ± 0.4	48.3 ± 1.5	39.9 ± 0.4	0	0	39.0 ± 2	61.0 ± 3
AR SA508 HT	0	0	12.5 ± 0.4	34 ± 1	53.5 ± 0.5	0	0	31.9 ± 1.6	68.1 ± 3.4
Cr Coated SA508	2 ± 0.6	27.1 ± 0.8	16.9 ± 6.7	17.4 ± 7	36.7 ± 1.8	2.6 ± 0.1	52.3 ± 2.6	18.9 ± 1	26.3 ± 1.3
Cr Coated SA508 HT	0.2 ± 0.06	34 ± 1	18 ± 7.2	9 ± 3.6	38.9 ± 1.9	3.3 ± 0.2	51.8 ± 2.6	16.1 ± 0.8	28.9 ± 1.5

Table 3
Percentage of Cr and Fe oxides with respect to metallic peaks measured using HAXPES 2p and 2s peaks for uncoated, Cr coated SA508 before and after heat treatment. The uncertainty represents the errors associated with peak fitting calculated from CASA XPS software.

	%Cr metal	%Cr Oxide	% Fe metal	% Fe Oxide	%Cr metal	%Cr Oxide	% Fe metal	% Fe Oxide
	Lower sampling depth (9 nm)				Higher sampling depth (30 nm)			
	Cr 1*s*		Fe 1*s*		Fe 2*p* Cr 2*s*			
AR SA508	0	0	19.7 ± 0.6	80.3 ± 2.4	0	0	39 ± 2	61 ± 3
AR SA508 HT	0	0	26.8 ± 0.8	73.2 ± 2.2	0	0	31.9 ± 1.6	68.1 ± 3.4
Cr Coated SA508	6.9 ± 0.2	93.1 ± 2.8	49.3 ± 19.7	50.7 ± 20.2	4.7 ± 0.2	95.3 ± 4.8	41.8 ± 2	58.2 ± 2.9
Cr Coated SA508 HT	0.4 ± 0.01	99.6 ± 3	66.7 ± 26.7	33.3 ± 13.3	5.9 ± 0.3	94.1 ± 4.7	35.7 ± 1.8	64.3 ± 3.2

Table 4
Bulk oxygen measurement of uncoated and Cr coated SA508 before and after heat treatment.

	As received	Cr coated
SA508	570 ppm	447 ppm
SA508 HT (50 °C 120 h)	594 ppm	454 ppm
Uncertainty in measurement	±52 ppm	

Table 5
Aerated density, Tap Density, Hausner ratio and Carr's index of uncoated and Cr coated SA508 powder.

	Aerated density, ρ_a (g/ml)	Tapped density, ρ_t (g/ml)	Hausner Ratio, HR	Carr's Index, CI
AR SA508	4.4 ± 0.03	4.9 ± 0.02	1.1 ± 0.01	10.9 ± 0.71
Cr coated SA508	4.4 ± 0.1	4.8 ± 0.11	1.1 ± 0.01	7.8 ± 0.10

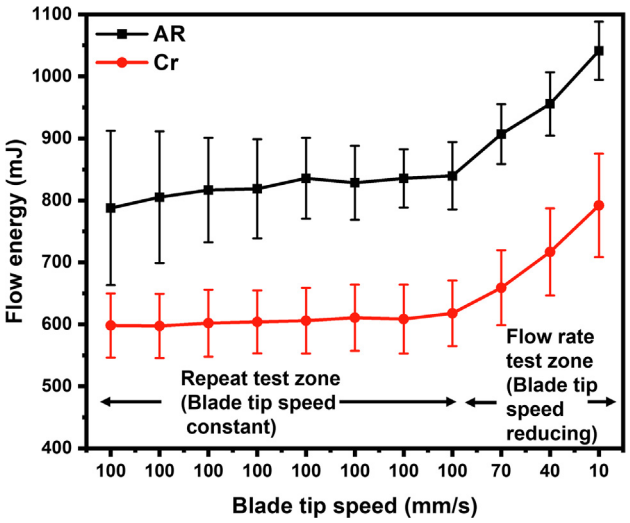

Fig. 9. Downward flow energy of powder as a function of blade tip speed for uncoated and Cr coated SA508 powder. The standard deviation is measured from 3 tests.

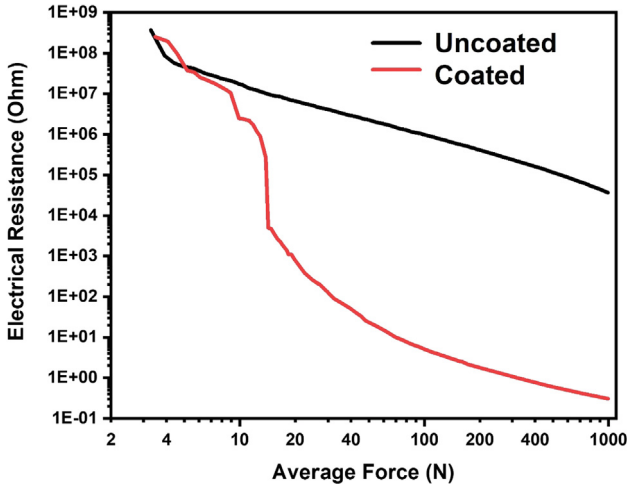

Fig. 10. Mean electrical resistance of uncoated and Cr coated SA508 powder as a function of applied force.

Table 6
Charge density of uncoated and Cr coated SA508 powder measured using Farady cage.

Sample	Charge density (nC/g)	
	Average	Std. Dev.
SA508 AR	−47.74	0.34
SA508 Cr Coated	−24.64	0.22

Since uncoated SA508 steel powder already has good flowability, surface coating may not significantly improve the final surface finish of additively manufactured product. However, this study demonstrates an alternate way to improve powder flowability by surface treatment of powder with a suitable coating.

4. Conclusions

A chromium film approximately 7 nm in thickness was deposited on a gas atomized SA508 Grade 3 low-alloy steel powder using magnetron sputtering with the aim of protecting the powder from

continued oxidation during storage. Coated and uncoated powders were then tested for their oxidation resistance as well as their flowability. XPS and HAXPES were utilised to confirm that continuous Cr films had formed, and to investigate oxygen pick-up in accelerated oxidation studies. In addition, electrical conductivity measurements were carried out to shed light on variations in flowability. The study has led to the following conclusions:

- Magnetron sputtering led to complete encapsulation of the powder with chromium, as confirmed by XPS.
- After accelerated oxidation experiments the near-surface oxygen concentration, as measured with HAXPES, was significantly lower for the chromium coated powder when compared to the uncoated powder. Bulk oxygen measurements also showed a slightly lower oxygen concentration in the Cr coated powder relative to the uncoated powder. Both analyses therefore demonstrate the benefit of depositing a thin film of Cr by magneton sputtering.
- Tribo-electric charging of the powder was reduced with a chromium coating. This could be due to a reduction in the thickness of the oxide layer and an increase in electrical conductivity on the surface of powder particles associated with the sputter-deposited chromium oxide film.
- The flowability of powder, as measured by the tapped density and a FT4 rheometer, was found to improve with a chromium coating. The improvement in flowability can be tailored to reduced tribo-electric charging, resulting in a lower cohesivity for the powder.

This study demonstrates that the oxidation of metallic powders can be mitigated without an inert atmosphere. This new approach could significantly reduce the costs associated with powder handling and storage. The study also suggests that it may be possible to improve material properties in additive manufacturing through the use of suitable coatings. Further work will address the effect of the Cr coating on the microstructure and mechanical properties of components manufactured by solid state processing. The effects of mechanical pre-treatments on the quality of coatings will also be considered.

Data availability

Data will be made available on request.

Declaration of Competing Interest

The authors declare that they have no known competing financial interests or personal relationships that could have appeared to influence the work reported in this paper.

Acknowledgements

This work was funded by MAPP: EPSRC Future Manufacturing Hub in Manufacture using Advanced Powder Processes EP/P006566/1. This work was also supported by the Henry Royce Institute for Advanced Materials, funded through EPSRC grants EP/R00661X/1, EP/S019367/1, EP/P025021/1 and EP/P025498/1. Rahul Unnikrishnan would also like to acknowledge EPSRC Grant EP/T016728/1.

Appendix A. Supplementary material

Supplementary data to this article can be found online at https://doi.org/10.1016/j.matdes.2022.110900.

References

[1] H.V. Atkinson, S. Davies, Fundamental aspects of hot isostatic pressing: An overview, Metall. Mater. Trans. A Phys. Metall. Mater. Sci. 31 (12) (2000) 2981–3000, https://doi.org/10.1007/s11661-000-0078-2.
[2] A.J. Cooper, R.J. Smith, A.H. Sherry, An Assessment of the Ductile Fracture Behavior of Hot Isostatically Pressed and Forged 304L Stainless Steel, Metall. Mater. Trans. A 48 (5) (2017) 2207–2221, https://doi.org/10.1007/s11661-017-4005-1.
[3] W. Wei, L. Wang, T. Chen, X. Duan, W. Li, Study on the flow properties of Ti-6Al-4V powders prepared by radio-frequency plasma spheroidization, Adv. Powder Technol. 28 (9) (2017) 2431–2437, https://doi.org/10.1016/j.apt.2017.06.025.
[4] A.D. Iams, J.S. Keist, L.A. Giannuzzi, T.A. Palmer, The Evolution of Oxygen-Based Inclusions in an Additively Manufactured Super-Duplex Stainless Steel, Metall. Mater. Trans. A 52 (8) (2021) 3401–3412, https://doi.org/10.1007/s11661-021-06311-8.
[5] A.J. Cooper, N.I. Cooper, J. Dhers, A.H. Sherry, Effect of Oxygen Content Upon the Microstructural and Mechanical Properties of Type 316L Austenitic Stainless Steel Manufactured by Hot Isostatic Pressing, Metall. Mater. Trans. A Phys. Metall. Mater. Sci. 47 (9) (2016) 4467–4475, https://doi.org/10.1007/s11661-016-3612-6.
[6] S. Terashima, H.K.D.H. Bhadeshia, Changes in toughness at low oxygen concentrations in steel weld metals, Sci. Technol. Weld. Join. 11 (5) (2006) 509–516, https://doi.org/10.1179/174329306X113299.
[7] A. Srivastava, L. Ponson, S. Osovski, E. Bouchaud, V. Tvergaard, A. Needleman, Effect of inclusion density on ductile fracture toughness and roughness, J. Mech. Phys. Solids 63 (1) (2014) 62–79, https://doi.org/10.1016/j.jmps.2013.10.003.
[8] E. Stavroulakis, S. Irukuvarghula, E. Pickering, D. Stewart, M. Preuss, Fundamental Aspects of Functional Grading via Powder Hot Isostatic Pressing - Development of microstructure and diffusional processes, Mater. Des. 215 (2022), https://doi.org/10.1016/j.matdes.2022.110437 110437.
[9] C.-O. Olsson, D. Landolt, Passive films on stainless steels- chemistry, structure and growth, Electrochim. Acta 48 (2003) 1093–1104, https://doi.org/10.1016/S0013-4686(02)00841-1.
[10] H. Karlsson, L. Nyborg, S. Berg, Surface chemical analysis of prealloyed water atomised steel powder, Powder Metall. 48 (1) (2005) 51–58, https://doi.org/10.1179/0032589005X37675.
[11] A. Eder, G.H.S. Schmid, H. Mahr, C. Eisenmenger-Sittner, Aspects of thin film deposition on granulates by physical vapor deposition, Eur. Phys. J. D 70 (11) (2016).
[12] A. Canakci, F. Erdemir, T. Varol, R. Dalmiş, S. Ozkaya, Effects of a new pre-milling coating process on the formation and properties of an Fe-Al intermetallic coating, Powder Technol. 268 (1) (2014) 110–117, https://doi.org/10.1016/j.powtec.2014.08.034.
[13] O. Güler, T. Varol, Ü. Alver, A. Çanakçı, The effect of flake-like morphology on the coating properties of silver coated copper particles fabricated by electroless plating, J. Alloys Compd. 782 (2019) 679–688, https://doi.org/10.1016/j.jallcom.2018.12.229.
[14] Y. He, A. Hassanpour, A.E. Bayly, Combined effect of particle size and surface cohesiveness on powder spreadability for additive manufacturing, Powder Technol. 392 (2021) 191–203, https://doi.org/10.1016/j.powtec.2021.06.046.
[15] S. Matsusaka, H. Maruyama, T. Matsuyama, M. Ghadiri, Triboelectric charging of powders: A review, Chem. Eng. Sci. 65 (22) (2010) 5781–5807, https://doi.org/10.1016/j.ces.2010.07.005.
[16] S. Matsusaka, Control of particle tribocharging, KONA Powder Part. J. 29 (29) (2011) 27–38, https://doi.org/10.14356/kona.2011007.
[17] T. Oguchi, M. Tamatani, Contact electrification phenomena and powder surface treatments, Wear 168 (1–2) (1993) 91–98, https://doi.org/10.1016/0043-1648(93)90202-W.
[18] C.N. Hulme, Flow behavior of magnetic steel powder, Part. Sci. Technol. 40 (5) (2022) 576–588.
[19] H.R. Verma, Atomic and nuclear analytical methods: XRF, mössbauer, XPS, NAA and ion-beam spectroscopic techniques. 2007. doi: 10.1007/978-3-540-30279-7.
[20] "User's Guide, QUASES: Quantitative Analysis of Surface by Electron Spectroscopy Version 5.1," QUASES-Tougaard, 2011.
[21] M.D. Abràmoff, P.J. Magalhães, S.J. Ram, Image processing with imageJ, Biophotonics Int. 11 (7) (2004) 36–41, https://doi.org/10.1201/9781420005615.ax4.
[22] H. Zhang, J. Poole, R. Eller, M. Keefe, Cobalt sputtering target and sputter deposition of Co thin films for cobalt silicide metallization, J. Vac. Sci. Technol. A Vacuum, Surfaces, Film. 17 (4) (1999) 1904–1910, https://doi.org/10.1116/1.581702.
[23] D.V. Sidelev, G.A. Bleykher, V.A. Grudinin, V.P. Krivobokov, M. Bestetti, M.S. Syrtanov, E.V. Erofeev, Hot target magnetron sputtering for ferromagnetic films deposition, Surf. Coatings Technol. 334 (2018) 61–70.
[24] B.F. Spencer, et al., Inelastic background modelling applied to hard X-ray photoelectron spectroscopy of deeply buried layers: A comparison of synchrotron and lab-based (9.25 keV) measurements, Appl. Surf. Sci. 541 (December 2020) (2021), p. 148635, doi: 10.1016/j.apsusc.2020.148635.
[25] A. Regoutz, M. Mascheck, T. Wiell, S.K. Eriksson, C. Liljenberg, K. Tetzner, B.A.D. Williamson, D.O. Scanlon, P. Palmgren, A novel laboratory-based hard X-ray photoelectron spectroscopy system, Rev. Sci. Instrum.nts 89 (7) (2018) 073105.

[26] D.J.H. Cant, B.F. Spencer, W.R. Flavell, A.G. Shard, Quantification of hard X-ray photoelectron spectroscopy: Calculating relative sensitivity factors for 1.5- to 10-keV photons in any instrument geometry, Surf. Interface Anal. 54 (4) (Apr. 2022) 442–454, https://doi.org/10.1002/sia.7059.
[27] N. Fairley, V. Fernandez, M. Richard-Plouet, C. Guillot-Deudon, J. Walton, E. Smith, D. Flahaut, M. Greiner, M. Biesinger, S. Tougaard, D. Morgan, J. Baltrusaitis, Systematic and collaborative approach to problem solving using X-ray photoelectron spectroscopy, Appl. Surface Sci. Adv. 5 (2021) 100112.
[28] Standard Test Method for Tap Density of Metal Powders and Compounds, ASTM Int, 2015, pp. 15–18, https://doi.org/10.1520/B0527-22.
[29] G. Xu, P. Lu, M. Li, C. Liang, P. Xu, D. Liu, X. Chen, Investigation on characterization of powder flowability using different testing methods, Experimantal Therm. Fluid Sci. 92 (2018) 390–401.
[30] D. Geldart, E.C. Abdullah, A. Hassanpour, L.C. Nwoke, I. Wouters, Characterization of powder flowability using measurement of angle of repose, China Particuology 4 (1990) (2006) 104–107.
[31] C. Hare, U. Zafar, M. Ghadiri, T. Freeman, J. Clayton, M.J. Murtagh, Analysis of the dynamics of the FT4 powder rheometer, Powder Technol. 285 (2015) 123–127, https://doi.org/10.1016/j.powtec.2015.04.039.
[32] D. Böhm, Resistance measurement for layer thickness determination on coated granular, media, Masters Thesis, TU, Vienna, 2017.
[33] Standard test for determining electrical ,conductivity using the electromagnetic (Eddy-Current) method, ASTM Int. (2009) 1–6, https://doi.org/10.1520/E1004-17.
[34] U. Zafar, F. Alfano, M. Ghadiri, Evaluation of a new dispersion technique for assessing triboelectric charging of powders, Int. J. Pharm. 543 (1–2) (2018) 151–159, https://doi.org/10.1016/j.ijpharm.2018.03.049.
[35] A.P. Long, S.L. Li, H. Wang, H. Chen, Characterization of oxide on the water-atomized FeMn powder surface, Appl. Surf. Sci. 295 (2014) 180–188, https://doi.org/10.1016/j.apsusc.2013.12.183.
[36] H. Shinotsuka, S. Tanuma, C.J. Powell, D.R. Penn, Calculations of electron inelastic mean free paths. X. Data for 41 elemental solids over the 50 eV to 200 keV range with the relativistic full Penn algorithm, Surf. Interface Anal. 47 (9) (Sep. 2015) 871–888, https://doi.org/10.1002/sia.5789.
[37] M.C. Biesinger, B.P. Payne, Resolving surface chemical states in XPS analysis of first row transition metals, oxides and hydroxides : Cr, Mn, Fe, Co and Ni, Appl. Surf. Sci. 257 (2011) 2717–2730, https://doi.org/10.1016/j.apsusc.2010.10.051.
[38] A. Ejigu, L. Le Fevre, B. F. Spencer, C. Bawn, and R. A. W. Dryfe, "An aqueous-based Secondary Aluminum-ion Battery," 2021.
[39] H. Chen, J. Li, P. Du, Z. Yu, C. Liu, Oxide film properties on an interstitial-free manganese alloyed steel in sodium sulphate solution, Int. J. Electrochem. Sci. 13 (5) (2018) 4085–4099, https://doi.org/10.20964/2018.05.81.
[40] A.L. Marasco, D.J. Young, The oxidation of Iron-Chromium-Manganese alloys at 900°C, Oxid. Met. 36 (1–2) (1991) 157–174, https://doi.org/10.1007/BF00938460.
[41] F.H. Stott, F.I. Wei, High temperature oxidation of commercial austenitic stainless steels, Mater. Sci. Technol. (United Kingdom) 5 (11) (1989) 1140–1147, https://doi.org/10.1179/mst.1989.5.11.1140.
[42] M. Krantz, H. Zhang, J. Zhu, Characterization of powder flow : Static and dynamic testing, Powder Technol. 194 (3) (2009) 239–245, https://doi.org/10.1016/j.powtec.2009.05.001.
[43] L. Marchetti, C. Hulme-Smith, Flowability of steel and tool steel powders: A comparison between testing methods, Powder Technol. 384 (2021) 402–413, https://doi.org/10.1016/j.powtec.2021.01.074.
[44] R.C. Ku, W.L. Winterbottom, Electrical conductivity in sputter-deposited chromoium oxide coatings, J. Thin Solid Film. 127 (1985) 241–256.